

TSUNAMI PRESSURE ON STRUCTURES DUE TO TSUNAMI INUNDATION FLOW

Tsutomu Sakakiyama¹

Pressure profiles acting on walls of 2D and 3D structures due to tsunami inundation flow were discussed. Mechanism of the tsunami pressure acting on these different types of structures was explained. Due to the water damming up in front of the 2D vertical wall, the maximum inundation depth is higher than that on wall of 3D structure when the Froude number is less than 2.8. The improved formula based on that by Asakura et al. (2002) was proposed to estimate the maximum inundation depth on 2D vertical wall as a linear function of the Froude number. Experimental results show the maximum inundation depth on the wall of 3D structure is evaluated from the energy conservation law for steady flow. Inundation depth, velocity and resultant Froude number of tsunami were also investigated with numerical simulation results. The effects of the bottom roughness on the inundation flow of tsunami is presented.

Keywords: tsunami; inundation depth; tsunami pressure; structure

INTRODUCTIONS

After the tsunami disaster due to the 2011 off the Pacific coast of Tohoku Earthquake, the design of tsunami evacuation buildings and protective walls in nuclear power plants is a matter of greater interest to us.

When considering a tsunami inundation flow, the maximum inundation depth on the wall of the structures is a critical factor and also a pressure profile is necessary to be evaluated.

Asakura et al.(2002) already proposed the experimental formula to estimate the maximum inundation depth as a function of the Froude number. However, their formula was based on experiments using both 2D and 3D structures and the data scatters ranging from -50% to +50%.

The guideline on tsunami evacuation buildings was issued by the Cabinet Office of Japan in 2005(Cabinet Office, Government of Japan, 2005). According to the guideline, the maximum inundation depth on a wall of structure is three times the maximum inundation depth without structures. The pressure profile on the wall is given by that of the hydrostatic pressure.

After the 2011 Tohoku-Oki tsunami disaster, that guideline was reviewed and the new document was released (NILIM, 2012). Still this official guideline gives the maximum inundation depth on structures as the function of the inundation depth without structures, not considering the effect of the velocity of the inundation flow. Guidelines or standards for design are usually simple. However, they should include basic principles.

On the other hand, in order to discuss the inundation depth more detailedly, there are several methods such as the experimental approach(Rueben et al, 2011; Park et al.,2013) or the numerical simulation one(Wu,1999; Sakakiyama,2010). After understanding the phenomena of the inundation flow, minimum requirements should be included in the design standard of the tsunami evacuation building and protective walls. The difference of the maximum inundation depth between 2D and 3D structures is not discussed yet.

The present work aims at showing first the mechanism of the difference of the maximum inundation depth between 2D and 3D structures. Second, the experimental formulae to estimate the maximum inundation depth on walls of the 2D and 3D structures are proposed. Pressure profiles on the wall of 2D and 3D structures are discussed using results of both experiments and numerical simulations.

INUNDATION FLOW NEAR 2D WALL AND AROUND 3D STRUCTURE

Experimental Method

Experiments were carried out using the 2D wave flume as shown in Fig. 1. The wave flume is 205m long, 6.0m deep and 3.4m wide. The bottom topography is not simple consisting of 1/11-, 1/100 and 1/50 uniform slopes. The existing topography model in the wave flume was exploited. The steepest slope of 1/11 was installed to make the water depth deep near the wave generator as $h_c=4.23\text{m}$.

Detail of the site model was shown in Fig. 2. The water depth at the seawall was 0.16m and the ground level(G.L.) is 0.04m above the still water level. Wave gages were set at several positions as shown in Figures 1 and Fig. 2. Current meters were at two locations, $x=-10\text{m}$ and -5m in the middle of the water depth, respectively. The data obtained at $x=-10\text{m}$ were used as the boundary condition for the numerical simulation. The axes of coordinates are defined in Fig. 2. Free surface displacement measured from $z=0$ is denoted by η . When discussing the inundation flow, the vertical axis z' is defined as $z'=z-\text{G.L.}$ and the inundation depth is denoted by ζ measured from the G.L.

¹ Fluid Dynamics Sector, Central Research Institute of Electric Power Industry, 1646 Abiko, Abiko-city, Chiba, 270-1194, Japan

lines covering a half-width of the front wall, at 0.05m interval from the center line to the corner except that the interval near the corner is 0.04m. The level of the pressure transducers ranges from 0.01m above the G.L. up to 0.19m at every 0.01m. The pressure measurement was carried out line by line because of the limitation of the pressure transducers available, that is, 19 sensors. The highest level of $z'=0.19\text{m}$ was decided by the observation of the run-up on the wall in preliminary experiments.

Side walls of the wave flume reflect flow from the structure. The positions of cubes were determined so that the side walls and the single cube make the flow regime a mirror image. The mirror image is true of the two cube case. The blockage ratio denoted by r_b which is defined by the ratio of a width of a structure to that of the flow is $r_b=0.5/3.4=0.147$ of case of a single cube and $r_b=0.5/1.7=0.294$ of the case of two cubes. The blockage ratio of a 2D structure is $r_b=1.0$.

The cube is high enough that overtopping is not allowed in the experiments.

2D numerical simulation

Since a 2D structure was not included in the experiments, a numerical simulation was conducted instead under the same tsunami condition to investigate differences of the inundation flow between 2D and 3D structures.

The numerical simulation code called CADMUS-SURF/3D (Arikawa et al., 2007) was used. This code is available for free with the open source. CADMUS-SURF/3D employs the porosity model for the permeable structure such as rubble mound breakwater in the governing and continuity equations for one-phase flow. The $k-\varepsilon$ turbulence model is included. The VOF method is used to trace free surface. The code was parallelized. Now it is used as the so-called Japanese standard in the coastal engineering to complement physical model tests.

The calculation domain ranges from $x=-10\text{m}$ to 1.0m in the horizontal direction and from $z=-0.36$ to 0.34m in the vertical direction in the wave flume as shown in Fig. 2. The 2D wall is set at $x=1.0\text{m}$.

The following mesh sizes were employed in the x -direction: from $x=-10\text{m}$ to -5m the mesh size is uniform as $\Delta x=0.05\text{m}$, from $x=-5\text{m}$ to 0m $\Delta x=0.05\text{m}$ to 0.01m increased in a geometric progression with the ratio $r=1.02$ and from $x=0\text{m}$ to 1.0m $\Delta x=0.01\text{m}$ uniform. The vertical mesh size Δz is uniform as $\Delta z=0.005\text{m}$.

The measured free surface displacement and velocity at $x=-10\text{m}$ were used as the boundary condition. Since the measured results include both the incident and reflected waves, any special treatment was not required to prevent multi-reflected waves at the boundary condition. The measured free surface displacement and velocity at $x=-5\text{m}$ were used to verify the numerical results as well as those on the site.

Comparison of flow around 2D and 3D structures

Figures 5 and 6 show the inundation flow around a single cube and multiple cubes, respectively. The tsunami is first dammed up by the seawall and runs down onto the site. There occurs a critical depth near the edge of the site resulting in the supercritical flow on the site. The flow with very smooth surface observed in the left part of each photograph indicates that the flow keeps supercritical. Blue part in the flow was visualized using dye. The Froude number defined by the flow condition without the structures is 1.5 when the maximum water depth $\zeta_0=0.073\text{m}$ and its simultaneous horizontal velocity $u=1.28\text{m/s}$. The flow runs up on the front walls of the single cube and that of the two cubes.

The water level behind the single cube is quite small. It means that less of the flow does not turn into the rear of the structure and it keeps the thin layer. Wake is not generated behind the structure in the supercritical flow.

Fig. 6 shows the inundation flow around multiple cubes. A gap between the front two cubes is narrower than that of the single cube test. Therefore, the difference between two cases is observed when comparing the flows between photographs at the bottom in Fig. 5 and Fig. 6. The contour of maximum water level around the single cube is round in front of the single cube and becomes rather straight along the stream making the shape of a horseshoe as the blue dye indicates. On the other hand, as the gap between two cubes becomes smaller, the gap is filled with the flow and the contour of the maximum water level make almost straight. As seen at the bottom photograph of Fig. 6 the edge of the reverse flow tends to be nearly straight. The phenomena is quite different from the edge configuration of the reverse flow from the single cube.

Figure 7 shows the numerical simulation results of the water level change in time and space near the 2D wall. Although the numerical simulation was carried out in the 2D field, the depiction of the water level in Fig. 7 is extended to the y direction in the 3D field in order to compare with the flow around the 3D structures of Figs 5 and 6. Until the inundation flow reaches the 2D wall, the flow

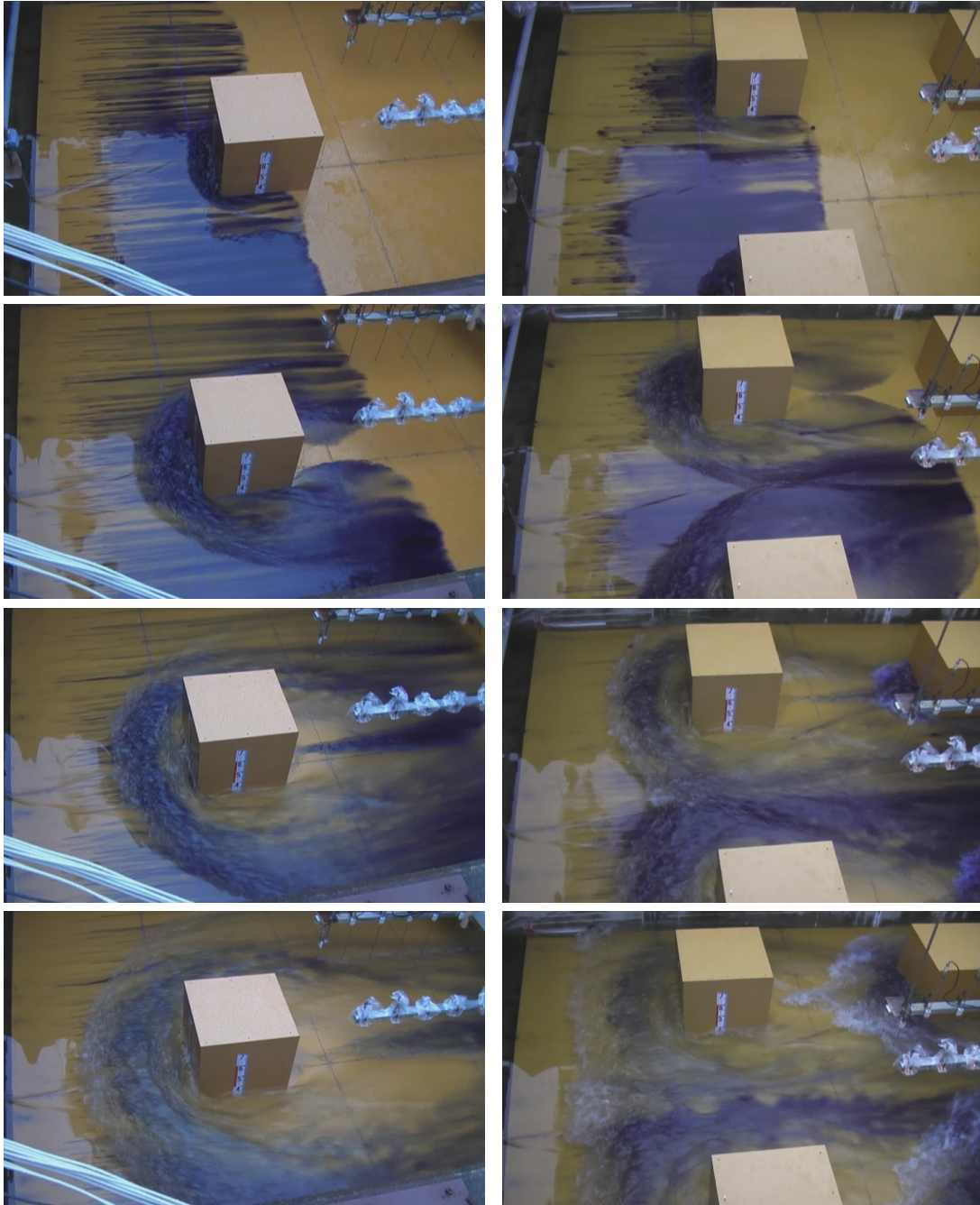


Figure 5: Inundation flow around a single cube (time interval is 1s, one side is 0.50m long)

Figure 6: Inundation flow around multiple cubes (time interval is 1s, one side is 0.50m long)

is same as that in the case of the 3D structures. Overtopping is not allowed in all three cases. The inundation flow is completely blocked by the 2D wall while the flow goes through the gap of the 3D structures. The run up height on the 2D wall keeps going up exceeding the maximum inundation depth on the 3D structure wall because the flow comes from the upstream and does not go downstream.

Figure 8 shows the water level changes in space and time. The water is dammed up by the seawall at $x=0$. Accompanying the critical depth near the seawall of the site, the inundation flow tends to the supercritical flow. It is dammed up again by the 2D wall. The flow is completely blocked there, runs up and the upper layer of the flow is reversed by the 2D wall.

Figure 9 shows a snap shot of the velocity field. At this moment when the water level on the wall is maximum the water just in front of the wall is nearly stagnant. Therefore, the pressure profile is considered to be hydrostatic in a case of the 2D structure.

In case of the 3D structures, there is a stagnation point on the front wall of the structure but the

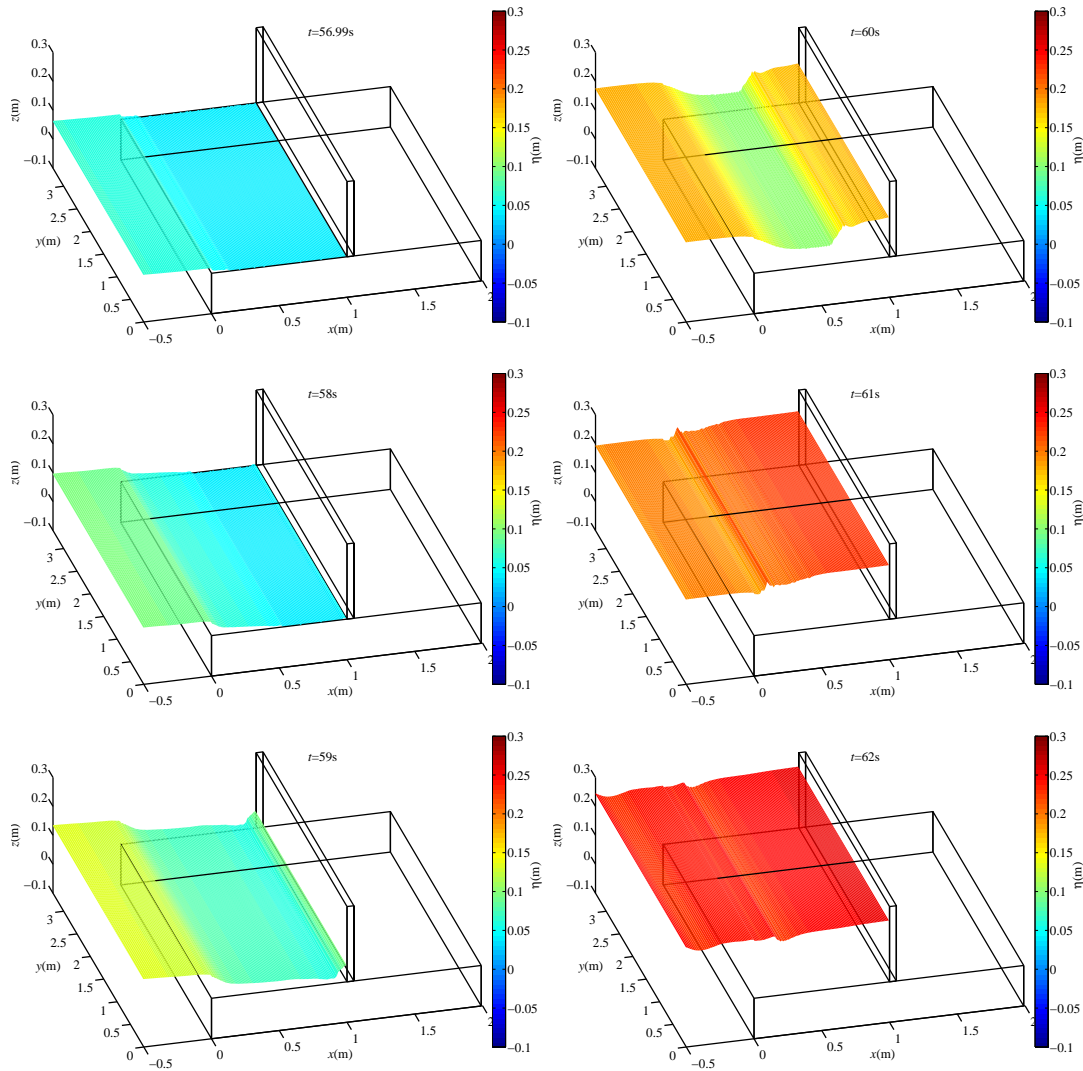


Figure 7: Water level of inundation flow near 2D wall

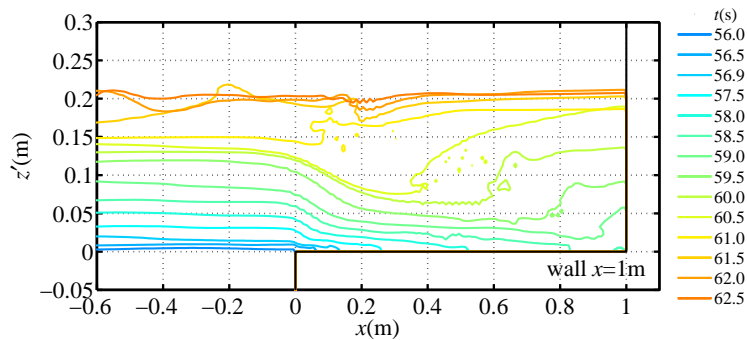


Figure 8: Free surface displacement in front of 2D structure.

flow is not stagnant on the whole area of the wall. There occur upward and downward currents along the wall. Those currents go around the structure and downstream. There is vertical distribution of the vertical component of the velocity on the wall. That causes the pressure deviation from that of the hydrostatic pressure. Pressure profile depends on the intensity of vertical component of velocity. That is the difference of the velocity field and resultant pressure profile between 2D and 3D structures.

Figure 10 shows the comparisons of the pressure profiles among three different structures featured with the blockage ratio, $r_b=0.147, 0.294$ and 1.0 . The pressure profiles were chosen when the horizontal

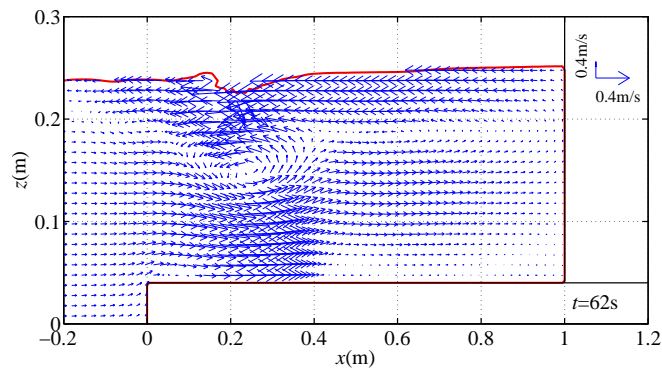


Figure 9: Velocity field and water level in front of 2D wall.

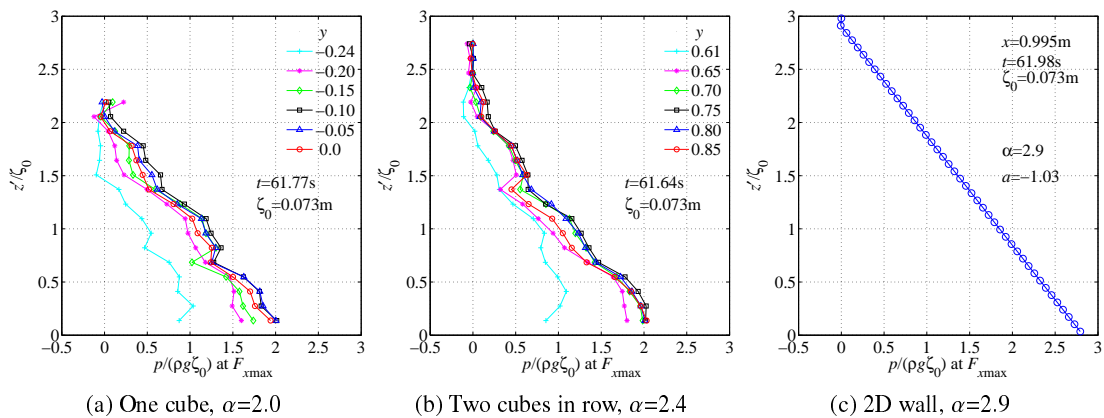


Figure 10: Pressure profiles and nondimensional maximum inundation depth α .

component of the fluid force was maximum denoted by F_{xmax} .

The pressure profiles were obtained from the center line to the edge on the front wall of the cubes. The red line with circle in Fig. 10(a) and (b) indicates the profile at the center line while the light blue line with a plus sign(+) that at to the edge. As Fig. 10(a) shows the pressure profile is somewhat uniform except that at the edge at the single cube. According to Fig. 10(b), the pressure at the edge at the two cubes is bigger than that of the single cube. The inundation depth at the edge of the structure in case of two cubes is higher than that in case of the single cube. This result agrees with the observation as shown in in Fig. 10.

The non- dimensional maximum inundation depth $\alpha = \zeta_w / \zeta_0$, the ratio of the maximum inundation depth on the wall ζ_w to that without the structure ζ_0 , were determined from the pressure profiles from the results of Fig. 10, $\alpha=2$ of a single cube, 2.4 of two cubes and 2.9 on the 2D wall. The non-dimensional maximum inundation depth increases as the blockage rate increases.

Once the maximum inundation depth is given, we need to specify the pressure profile for the design of structure walls.

The pressure profile of the 2D is simply given as hydrostatic pressure, as mentioned before, the flow near the 2D wall becomes stagnant.

Those on the wall of the 3D structures are also very close to hydrostatic pressure according to the experimental results of Fig. 10(a) and (b). However, these results are obtained under the specific condition of which the Froude number of the inundation flow is 1.5. Flow field around the 3D structure is not as simple as that near the 2D wall. The pressure profile should be more complicated, if the Froude number of the inundation flow increases. It seems that the Froude number 1.5 is not large enough to deform the pressure profile from the hydrostatic pressure.

NUMERICAL EXPERIMENTS FOR INUNDATION DEPTH ON 2D WALL

Numerical simulation

In order to propose an experimental formula for estimating the maximum inundation depth on the 2D structure, additional numerical simulation was carried out. To amass data on the inundation depth on the structure, the numerical simulation is powerful tools of which results were already veri-

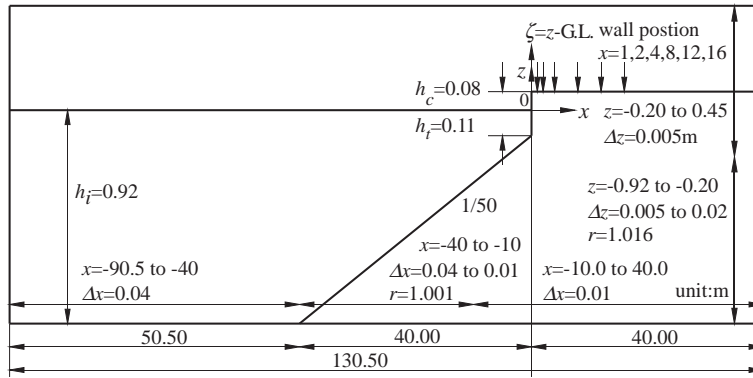


Figure 11: Calculation domain modified after Asakura et. al(2002)

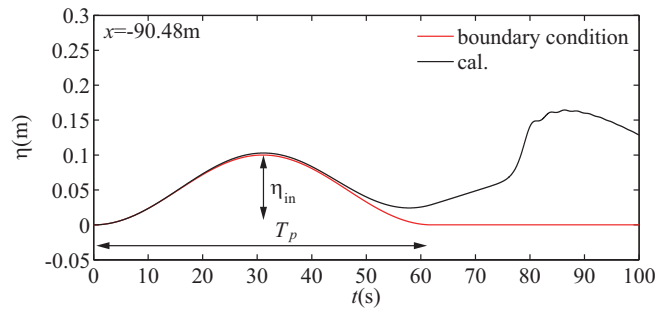


Figure 12: Boundary condition of free surface displacement and calculated result.

| | | |
|-----------------|----------------------|--|
| η_{in} (m) | 0.08, 0.10, 0.12 | |
| T_p (s) | 21, 42, 62 | |
| k_s (m) | 0.0001, 0.002, 0.005 | + smooth rough turbulent flow turbulent flow |

fied(Sakakiyama, 2010).

Figure 11 shows the set-up for numerical simulation for the purpose. This calculation condition was made based on the experimental conditions by Asakura et al.(2002). The calculation domain is 130.50m long and 1.37m deep. It is longer than the wave flume length in Asakura et al.(2002) because multi-reflection waves were observed in a preliminary calculation and it is crucial to prevent them from running up on the site.

Grid mesh sizes were shown in Fig. 11. In the following regions, the uniform and variable mesh were employed; from $x=-90$ to -40 m, a uniform mesh of $\Delta x=0.04$ m, from $x=-40$ to -10 m, variable mesh of $\Delta x=0.04$ m to 0.01 m with a ratio $r=1.001$ of a geometric progression. and from $x=-10$ to 40 m, a uniform mesh of $\Delta x=0.01$ m. Vertical mesh size are as follows; from $z=-0.92$ to -0.20 m, variable mesh of $\Delta z=0.02$ m to 0.005 m and from $z=-0.20$ to 0.045 m, a uniform mesh of $\Delta z=0.005$.

In the current numerical simulation, the 2D wall was set at $x=1, 2, 4, 8, 12$ and 16 m in total six positions. The origin of x -axis is set at the sea wall and that of z at the still water level. This aimed at investigating the effects of the Froude number on the pressure on the walls. It is expected that the inundation flow condition featured by the Froude number changes as it propagates on the site.

Figure 12 shows an example of the time histories of water level of tsunami. Red curve shows the time history of water level at the boundary condition. Black curve shows that of the calculated one. The reflected wave coming from the seawall is observed in Fig. 12. Calculations were aborted just before the multi-reflection wave reached the seawall.

Table.1 shows the calculation conditions. Combinations of the maximum water level η_{in} , the half period T_p and the bottom roughness length k_s give a calculation conditions. According to the parameters, case name was given as i.e., e10p62k01 indicating $(\eta_{in}, T_p, k_s)=(0.10\text{m}, 62\text{s}, 0.001\text{m})$. Calculations under the smooth turbulent condition were also carried out of which case name are denoted by k00 such as e12p42k00.

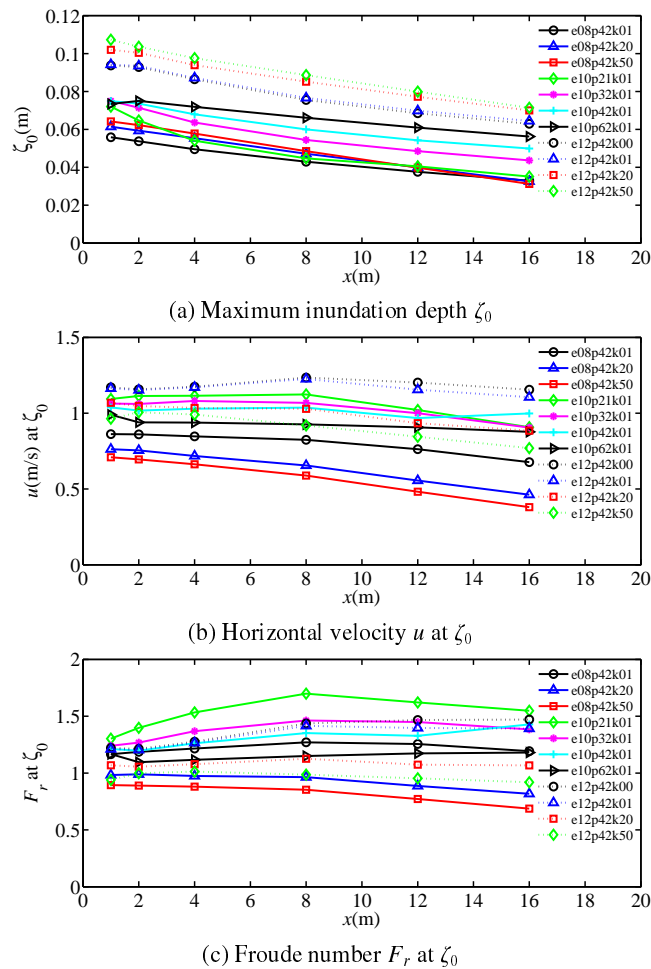


Figure 13: Spatial change of maximum inundation depth ζ_0 , horizontal velocity u and Froude number F_r

Results of inundation flow

Figure 13 shows spatial changes of the maximum inundation depth ζ_0 (Fig. 13(a)), the simultaneous horizontal component of the depth-averaged velocity u (Fig. 13(b)) and the Froude number F_r (Fig. 13(c)), where u and F_r are the values obtained at the same time of ζ_0 . Even if the boundary conditions of the tsunami are same such as case e08p42k01, e08p42k20, e08p42k50, the maximum inundation depth at $x=1$ m varies as shown in (Fig. 13(a)). This is explained by the effect of the bottom friction on the tsunami propagation from the offshore boundary to the seawall. As the bottom roughness k_s increases, the maximum water level at the seawall ($x=0$) increases. The bottom friction affects the energy flux more than the dissipation of the wave height. As the inundation flow propagates on the site, the maximum inundation depth ζ_0 decreases but the horizontal velocity does not show such a simple trend. According to the combination of ζ_0 and u , the Froude number of the inundation flow fluctuates slightly in the x -direction as shown in Fig. 13(c).

Figure 14 shows a comparison of the numerical simulation results of the configuration of the inundation flow. Fig. 14(a) shows the inundation flow without the wall and Fig. 14(b) that with the wall at $x=16$ m. Due to the existence of the seawall the tsunami is dammed up at the offshore side, $x=0$ m as it's running up on the ground of the site. The supercritical flow takes places after running down on the seawall.

In Fig. 14(b), just after the flow front touched the wall the run up with the thin water layer is observed on the wall at $t=64$ s. The momentum at the flow front is large and an impulsive pressure could occur. The inundation flow is dammed up by the 2-D wall and from $t=64$ to 76 s the flow started returning offshore. It is confirmed that an impact pressure does not exceed the pressure at the maximum water level.

Figure 15 shows the time histories of the inundation depth ζ , the depth-averaged horizontal velocity u_m and the specific energy E at $x=2$ m and 16 m, respectively. The vertical dashed lines indicate the times

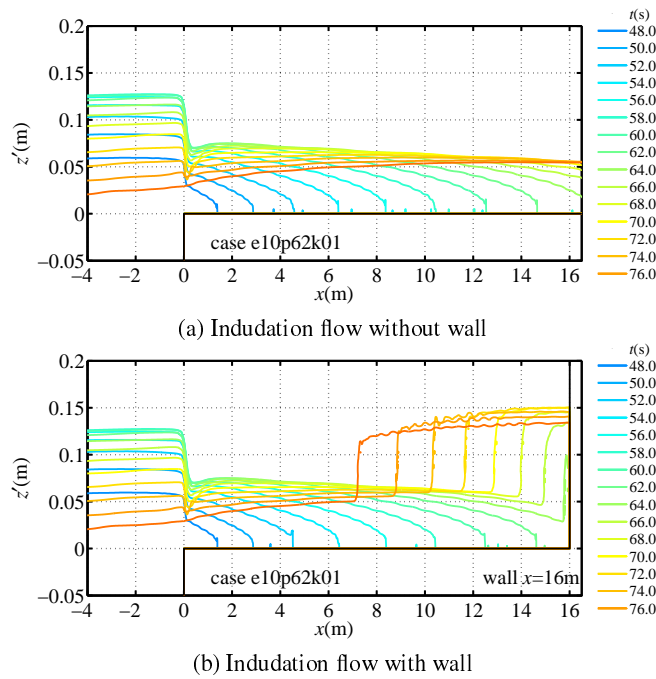


Figure 14: Profile change of inundation flow (case e10p21k01, $\eta_{in}=0.10m$, $T_p=62s$, $k_s=0.0001m$)

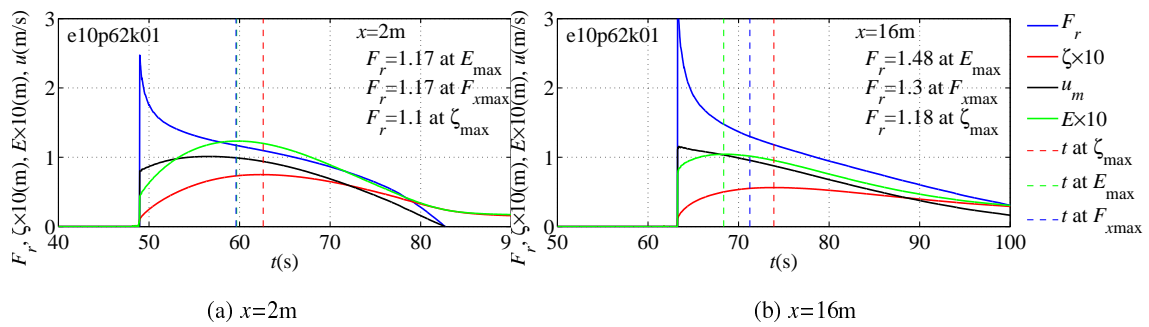


Figure 15: Inundation depth, velocity and specific energy(e10p62k01)

when the peak values took place of the specific energy, the inundation depth and the horizontal velocity, respectively. The specific energy E is given by the Eq. (1). While the inundation depth ζ at both $x=2m$ and $16m$ gradually increases in time, the horizontal velocity shows drastic change in its time history between $x=2m$ and $16m$. The maximum inundation depth decreases as the inundation flow propagates on land from $x=2m$ to $16m$. The maximum velocity at $x=2m$ occurs while that occurs at the current front at $x=16m$. This is due to the bottom friction.

$$E = \zeta + u^2/(2g) \tag{1}$$

The Froude number is defined at three phases, at the maximum of the specific energy, of the fluid force and of the inundation depth. The Froude number at the time when the maximum fluid force F_{xmax} is obtained after the numerical simulation with the wall was carried out. Therefore, from the point of view of predicting tsunami pressure or force, The Froude number at the maximum fluid force is not practical but in order to understand the phenomena of the tsunami force acting on the structure, the timing of the maximum force is included.

As the inundation flow propagates inland, the maximum inundation depth decreases, the simultaneous horizontal velocity increase and the resultant Froude number at the maximum specific energy increases. That occurs due to the change in the phase.

Theoretical consideration on inundation depth on wall

In order to reconsider the factor of three and the constant factors in the new guidelines by NILIM(2012), a basic theoretical consideration is described as follows: The inundation flow can be assumed as the

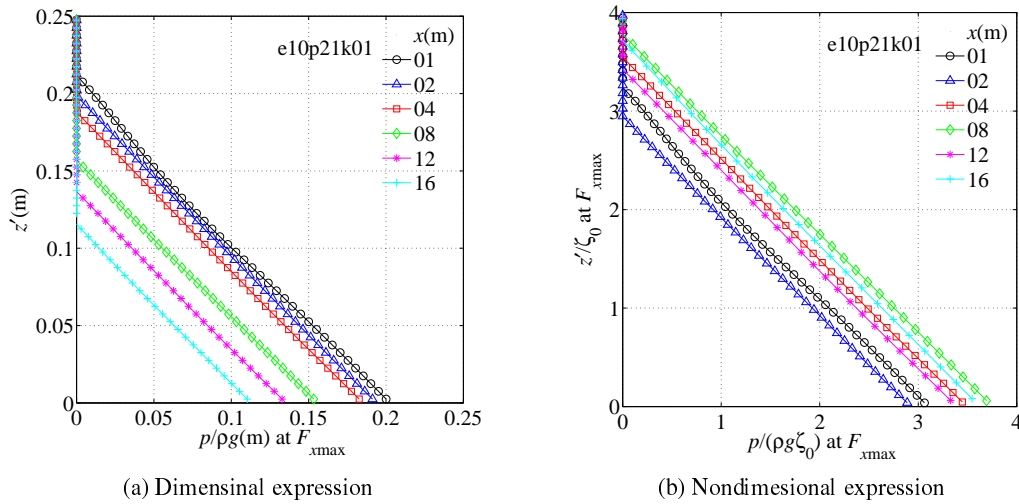


Figure 16: Profiles of maximum pressure z (case e10p21k01, $\eta_m=0.10\text{m}$, $T_p=62\text{s}$, $k_s=0.0001\text{m}$)

steady flow because tsunami has long wave period. From the energy conservation law given by Eq. (2), we can obtain a simple relationship between the inundation depth of tsunami without a structure and that on the structure wall as follows:

$$\frac{u^2}{2g} + \frac{p}{\rho g} + \zeta = \text{const.} \quad (2)$$

The values in the field without structures are denoted by the suffix “0” and those on the wall of structure denoted by the suffix “w”. The horizontal velocity u_w on the wall of the structure is null as $u_w=0$. On the free surface where it is one of streamlines, $p = 0$, Eq. (2) gives the following result.

$$\frac{u_0^2}{2g} + \zeta_0 = \zeta_w \quad (3)$$

The non-dimensional maximum inundation depth $\alpha = \zeta_w/\zeta_0$ is expressed by a quadratic function of the Froude number.

$$\alpha = \frac{\zeta_w}{\zeta_0} = 1 + \frac{u_0^2}{2g\zeta_0} = 1 + \frac{1}{2}F_r^2 \quad (4)$$

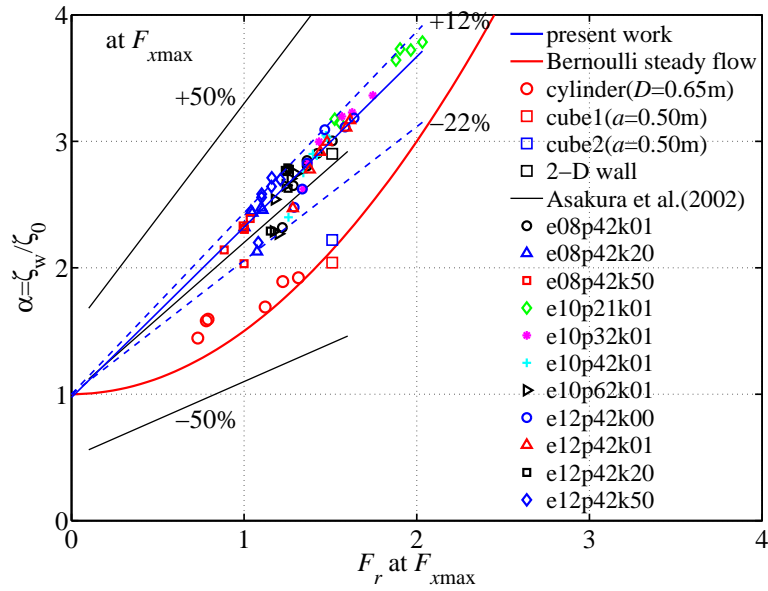
It is already confirmed that Eq. (4) is valid for cylindrical structure such as oil tanks (Sakakiyama et al., 2009). The question is whether Eq. (4) is valid for the 2D wall or not.

Results of maximum inundation depth and pressure profile

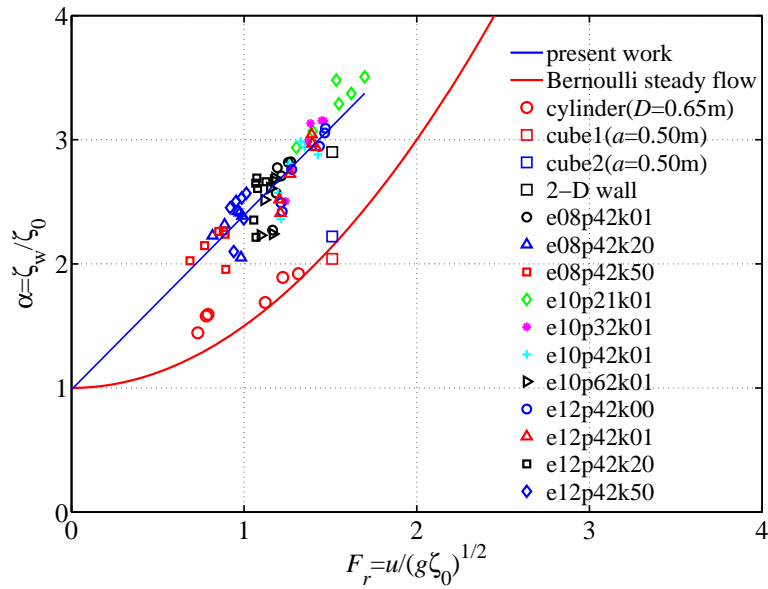
Figure 16(a) shows dimensional pressure profiles of at different positions of the 2D wall at $x=1, 2, 4, 8, 12$ and 16m . The horizontal axis shows the pressure head $p/(\rho g)$. These profiles show a simple trend: the maximum pressure and the maximum inundation depth decrease as the wall position changes from $x=1\text{m}$ to 16m . It simply means that as the inundation flow propagates into land, the maximum inundation depth decreases. However, the non-dimensional profiles are not so simple as the dimensional one. The non-dimensional profiles are not in order of the distance of the wall position. The Froude number does not change monotonously as the inundation flow propagates toward inland shown in Fig. 13(c). It is mainly due to the bottom friction. The maximum inundation depth decreases as it travels toward inland. Therefore, the maximum water level on the wall decreases. However, its velocity increases. At $x=1.0\text{m}$, pressure profile is not linear. The non-dimensional maximum inundation depth $\alpha = \zeta_w/\zeta_0$ in Fig. 16(b) exceeds three. Three times the maximum water level of inundation flow was the factor firstly recommended in the guideline of tsunami evacuation buildings (Cabinet Office, Government of Japan, 2005).

All results on the maximum inundation depth obtained by the present experiments, numerical simulations are shown in Fig. 17(a). The results of the 3D structures including results of cylindrical structure ($D=0.65\text{m}$) by Sakakiyama et al. (2009) are also plotted to compare with those of the 2D wall.

First, focusing on the results of the 3D structures of cubes and the data on cylinders with $D=0.65\text{m}$ with the red hollow circle (Sakakiyama et al., 2009), they are very close to the curve given by Eq. (4) identified with “Bernoulli steady flow” in the legend.



(a) Relationship α and F_r defined at F_{xmax} for analyzing data



(b) Relationship α and F_r defined at ζ_0 for experimental formula

Figure 17: Relationship between non-dimensional maximum inundation depth α and Froude number F_r .

The relationship between α and F_r of the experimental formula by Asakura et al.(2002) given by Eq. (5) is presented with black lines with its error ranges of $\pm 50\%$. Again, this experimental formula was obtained using both 2D and 3D experimental results. It is valid up to $F_r=1.6$.

The results for the 2D wall show a quite different trend from that of the 3D structure. Although there is some scatter in the data from -22% to 12% of which range is much smaller than $\pm 50\%$, a linear function can be obtained as expressed with Eq. (6). This data range is not an error but due to the effect of the bottom friction on the inundation flow as explained on Fig. 13.

$$\alpha = 1.0 + 1.2F_r (\pm 50\%) \quad (0.1 \leq F_r \leq 1.6) \quad (5)$$

$$\alpha = 1.0 + 1.4F_r (-0.22\% \sim 12\%) \quad (0.0 \leq F_r \leq 2) \quad (6)$$

The important point is that the inundation depth on the 2D wall is higher than that of the 3D structure when the Froude number is less than about 2 and a half. After the linear relationship was

proposed by the author (Sakakiyama, 2012), Ikeya et al. (2013) proved that this linear function was theoretically obtained from the momentum and continuity equations based on the one dimensional flow.

CONCLUSION

The present work described the tsunami inundation flow around the 3D structures comparing with the flow in front of the 2D wall. The difference of the maximum inundation depth on the walls was also presented between the 2D and 3D structures as well as profiles of the pressure acting on the walls. Primary conclusions are as follows.

1. The maximum inundation depth differs between 2D and 3D structures because of the differences of mechanism of the run-up on the walls and of flow pattern near the structures.
2. Proposed was the experimental formula to estimate the maximum inundation depth on the 2D wall as a linear function of the Froude number.
3. The maximum inundation depth on wall of the 3D structure is estimated by the Energy conservation law for the steady flow which is a quadratic function of the Froude number.
4. The maximum inundation depth on the 2D structure is higher than that on the 3D structure when the Froude number is less than about 2.8.
5. The pressure profile on the 2D wall due to the inundation flow is approximated by the hydrostatic pressure because the inundation flow is stagnant in front of the 2D wall.
6. The pressure profile on the 3D structure is not necessary approximated by the hydrostatic pressure, although the profiles obtained by the present experiments show nearly the hydrostatic pressure when the Froude number is about 1.5.

The differences of the maximum inundation depth and the pressure profile between the 2D and 3D structures are described and the formulae were proposed for the maximum inundation depth for these typical conditions. For the practical use, it is requires to estimate the maximum inundation depth for an arbitrary width of the structure or an arbitrary blockage ration. It should be done as a future work. Profile of pressure on a wall of 3D structure should be also investigated under the condition of higher Froude number.

REFERENCES

- Asakura, R., K. Iwase, T. Ikeya, M. Takao, T. Kaneto, N. Fuji, and M. Ohmori. 2002. The tsunami wave force acting on land structure, *Proc. of 28th Int. Conf. on Coastal Engineering*, ASCE, pp.1191-1202.
- Arikawa, T., T. Yamano, and M. Akiyama. 2007. Advanced Deformation Method of Breaking Waves by Using CADMAS-SURF/3D, *Annual Journal of Coastal Engineering*, JSCE, Vol. 54, pp.71-75(in Japanese).
- Cabinet Office, Government of Japan. 2013. Guideline on tsunami evacuation buildings, 73p.
- Ikeya, T., Y. Akiyama, and N. Iwamae. 2013. On the hydraulic mechanism of sustained tsunami wave pressure acting on land structures, *Journal of JSCE, Ser. B2(Coastal Engineering)*, Vol.69, No.2, pp.I_816-I_820(in Japanese).
- National Institute of Land and Infrastructure Management. 2012. Practical Guide on Requirement for Structural Design of Tsunami Evacuation Buildings, pp.I-7-I-17(in Japanese).
- Park, H., D.T. Cox, J.P. Lynett, D.M. Wiebe, and S. Shin. 2013. Tsunami inundation modeling in constructed environments: A physical and numerical comparison of free-surface elevation, velocity, and momentum flux, *Coastal Engineering*, Vol.79, pp.9-21.
- Rueben, M., R. Holman, D. Cox, S. Shin, J. Killian, and J. Stanley. 2011. Optical measurements of tsunami inundation through an urban waterfront modeled in a large-scale laboratory basin, *Coastal Engineering*, Vol.58, pp.229-238.
- Sakakiyama, T., S. Matsuura, and M. Matsuyama. 2009. Tsunami force acting on oil tanks and buckling analysis for tsunami pressure, *Journal of Disaster Research*, Vol.4, No.6, pp.427-434.
- Sakakiyama, T. 2010. Verification of numerical simulation model CADMAS-SURF/3D for tsunami acting on structures, *Annual Journal of Civil Engineering in the Ocean*, Vol.26, JSCE, pp.285-290.(in Japanese)

- Sakakiyama, T. 2012. Tsunami inundation flow and tsunami pressure on structures, *Journal of JSCE, Ser. B2(Coastal Engineering)*, Vol.68, No.2, pp.I_771-I_775(in Japanese).
- Wu, T.R. 2004. A numerical study of three-dimensional breaking wave and turbulence effects, Doctoral thesis, Cornell University, 265p.